J Appl Electrochem (2011) 41:1425–1431
DOI 10.1007/s10800-011-0366-0

ORIGINAL PAPER

Morphology-controlled synthesis and electrocatalytic characteristics of platinum structures on micro-patterned carbon nanotube platforms

Cheng Ai Li · Kwi Nam Han · Minh-Phuong Ngoc Bui · Xuan-Hung Pham · Myung Hyo Hong · Muhammad Irfan · Yong Shin Kim · Gi Hun Seong

Received: 9 August 2011 / Accepted: 29 October 2011 / Published online: 11 November 2011

Abstract In this study, platinum particles were fabricated on flexible, transparent, single-walled carbon nanotube films without the addition of reducing or protecting agents using a facile and controllable electrochemical method. Spherical platinum particles (SPPs) were transformed into flower-like platinum particles (FPPs) by varying the applied potential, the pattern size of the photoresist polymer, and the deposition time. An analysis of the X-ray diffraction data revealed that the FPPs possessed a face centered cubic structure. The intensity ratio of (111) to (200) diffraction lines for the FPPs (2.15) was greater than that of the SPPs (1.44), indicating that the as-prepared FPPs were dominated by the lowest-energy (111) facets. The electrocatalytic activities of the synthesized particles with regard to methanol and formic acid oxidation were investigated. The FPPs exhibited higher catalytic performance for the electrochemical oxidation of methanol and formic acid than the SPPs. The high oxidation current of the FPP-based electrode was directly related to the morphologies of the platinum particles. The simple approach employed in this study will be useful for fabricating particles of other noble metals with different morphologies.

Keywords Platinum particles · Single-walled carbon nanotube · Electrochemical synthesis · Electrocatalyst · Micro-patterning

1 Introduction

Metal particles have been intensively investigated for various applications due to their desirable electrical, optical, and catalytic properties [1–4]. Among these particles, platinum has attracted considerable interest because of its unique catalytic properties. For example, platinum particles serve as catalysts in the production of hydrogen [5] and in the reduction of pollutant gases emitted from automobiles [6]. Platinum particles are also used as electrocatalysts in electrode layers of proton exchange membrane fuel cells [7]. Extensive efforts have been devoted to the production of platinum catalysts with large surface areas to achieve high catalytic performance and platinum utilization [8–10]. Because of the strong dependence of physical and chemical properties on particle morphology, the ability to effectively control the platinum particle morphology may provide a significant opportunity for improving catalytic properties [11]. Therefore, platinum particles with a wide variety of morphologies, such as tetrahexahedrons [12], cubes [13], nanotubes [14], nanosponges [15], nanoflowers [16, 17], multi-armed or star-shaped nanocrystals [18, 19], and porous or dendritic structures [20–23] have been synthesized using numerous techniques. However, most of these structures are fabricated using wet chemical methods that involve the use of organic surfactants, polymeric stabilizers, and morphology-controlling agents at elevated temperatures. As such, impurities that disturb or limit the applications of metallic nanostructures on platinum surfaces may exist [24–26]. Electrochemical deposition is a

Electronic supplementary material The online version of this article (doi:10.1007/s10800-011-0366-0) contains supplementary material, which is available to authorized users.

C. A. Li · K. N. Han · M.-P. N. Bui · X.-H. Pham · M. H. Hong · M. Irfan · G. H. Seong (✉)
Department of Bionano Engineering, Hanyang University, Ansan 425-791, Korea
e-mail: ghseong@hanyang.ac.kr

Y. S. Kim
Department of Applied Chemistry, Hanyang University, Ansan 425-791, Korea

viable alternative technique for the preparation of platinum particles due to its simplicity, low cost of implementation, and the ability to directly deposit particles in desirable electrode locations [27–29].

Single-walled carbon nanotubes (SWCNTs) have been the focus of significant research as promising electrode materials due to their remarkable electrical, mechanical, thermal, and optical properties [30–32]. Due to these outstanding properties, SWCNT films have been employed as a new class of optically transparent and electrically conductive materials in electronics, catalysis, and sensing applications [33–36]. To fabricate and assess the utility of nanoparticle/carbon nanotube hybrid devices, research efforts have focused on the use of novel metal nanoparticles for the modification of electrode surfaces to enhance the electrocatalytic activity of electrodes. To develop nanoparticle/carbon nanotube hybrid devices, it is necessary to fabricate well-defined micro/nanostructures at defined positions on SWCNT films while maintaining large-scale control of their locations and orientations. Such a process insures excellent electrical contact, reliability, and reproducibility of the devices.

Here, a facile and controllable electrochemical process for fabricating three-dimensional (3D) flower-like platinum particles (FPPs) on flexible, transparent SWCNT films without the addition of a reducing or protecting agent is detailed. The shapes and sizes of the platinum particles were controlled by adjusting the applied potential and the pattern size of the photoresist polymer. The particles were analyzed using field emission-scanning electron microscopy (FE-SEM), transmission electron microscopy (TEM), and X-ray diffractometry (XRD). Furthermore, the effects of particle shape and size on the electrocatalytic properties of the fabricated platinum particles were characterized using cyclic voltammetry and chronoamperometry.

2 Experimental

SWCNT (Topnanosys Co., South Korea) films were fabricated on flexible poly(ethylene terephthalate) (PET) substrates using a vacuum filtration method [37]. A standard photolithography process was employed to generate a photoresist polymer template (AZ4620) on the SWCNT film surface [29]. Platinum particles were electrochemically deposited on pre-patterned SWCNT films in a 2.5 mM H_2PtCl_6 solution, which were prepared in 0.2 M H_2SO_4 (Fig. 1). Cyclic voltammetry (CV) and chronoamperometry measurements were performed with a CHI600C electrochemical analyzer. A clean platinum wire, an Ag/AgCl electrode (saturated in 3 M NaCl), and a platinum particle-modified SWCNT electrode were used as

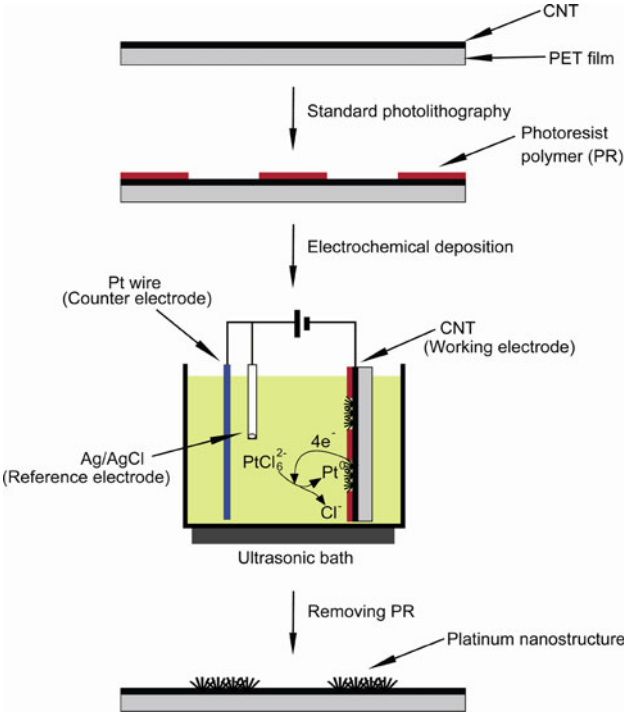

Fig. 1 Schematic of the patterning process for platinum structures electrochemically deposited on SWCNT films

the counter, reference, and working electrodes, respectively. All potentials were recorded versus the reference electrode. The solution was ultrasonicated during electrochemical deposition. The SWCNT electrodes were then immersed in a tetrahydrofuran solution to completely remove the photoresist polymer from the SWCNT electrodes. This step was followed by washing with ethanol and deionized water. The amount of deposited platinum particles was determined by Faraday's law. The morphology and structure of the platinum particles were characterized using FE-SEM (Hitachi S-4800, operating at 15 kV) and TEM (JEOL JEM-2100F, operating at 200 kV). The crystal structures of the platinum particles were analyzed with a D-Max 2500/PC (Rigaku Co., Japan) diffractometer with Cu Kα radiation.

The electrochemical properties of the platinum particle-based SWCNT electrodes were investigated using CV and chronoamperometry measurements in a standard three-electrode system at room temperature. The electrolyte solutions were composed of 0.25 M methanol or 0.25 M formic acid in 0.5 M H_2SO_4. Prior to the experiments, the solution was deoxygenated with high purity nitrogen gas. CVs for methanol and formic acid were performed in the range of -0.2 to 0.9 V and -0.2 to 1.0 V, respectively, at a sweep rate of 50 mV s^{-1}. Chronoamperometry curves for methanol oxidation and formic acid oxidation were measured at 0.6 and 0.4 V, respectively.

3 Results and discussion

Large-area SWCNT thin films were fabricated on transparent, flexible PET substrates using a vacuum filtration method. The thicknesses of the SWCNT films were controlled to ~100 nm by adjusting the concentration and volume of the SWCNT suspension. The average resistivity and transparency of the fabricated flexible SWCNT films were 350 ohm/sq and 80%, respectively (the transparency of the PET substrate was 89%). The SWCNT films exhibited a high degree of flexibility with a negligible change in resistivity upon hard bending. FE-SEM imaging of the SWCNT films revealed that the ordered SWCNTs were well-connected and formed a random and homogeneous film on the PET substrate (inset of Fig. 2a). To fabricate platinum particles on the SWCNT films, a photolithography method was employed to create well-defined photoresist polymer patterns. Such a process facilitates the electrochemical deposition of platinum particles on the SWCNT surface because of the sufficient electric field strength induced by the pattern features [38]. The photolithography approach employed in this study made it possible to create selective, stable, controllable, and homogeneous distributions of platinum particles on the SWCNT films (Fig. 2a). Clear patterns on the SWCNT films demonstrate the effectiveness of platinum particle patterning using this method. The excellent compatibility of the SWCNTs with the photolithography process allows for the fabrication of precise, high-resolution features [39]. The high magnification FE-SEM image in Fig. 2b illustrates that a large number of particles with diameters in the range of 200–400 nm were homogeneously distributed on the SWCNT film. Furthermore, these particles had a 3D flower-like appearance with folded surface microstructures composed of two-dimensional nanoflakes (inset of Fig. 2b). Figure 2c shows a typical TEM image of FPP morphology, which is consistent with the FE-SEM image in inset of Fig. 2b. The high-resolution TEM image of the area indicated by the black square in Fig. 2c is displayed in Fig. 2d. The nanoflake has grown anisotropically along the <111> direction, and the distance between the (111) planes is 0.225 nm, which is in agreement with that found for bulk platinum crystal.

The shape and size of the fabricated platinum microstructures exhibited a strong dependence on the applied potential and pattern size of the photoresist polymer. As

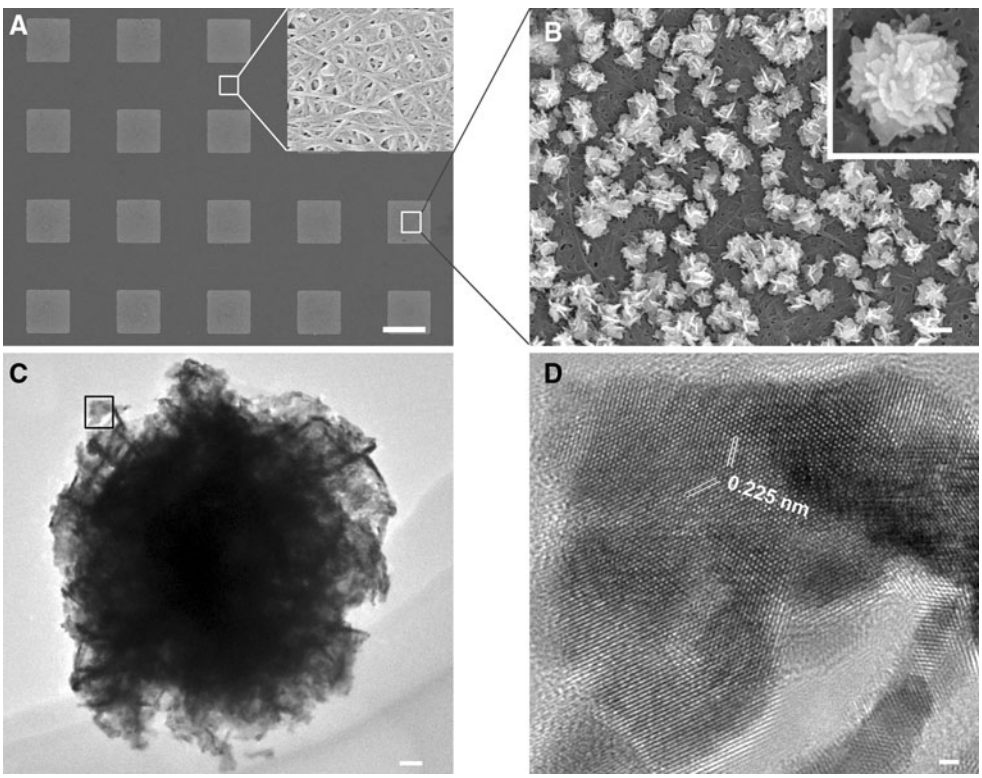

Fig. 2 **a** FE-SEM image of SWCNT films patterned with platinum particles. The *inset* is FE-SEM image of pristine SWCNT films protected with photoresist polymer. **b** FE-SEM image of electrochemically fabricated platinum particles. The *inset* is a high magnification image of a platinum particle on a SWCNT film. **c** TEM image of flower-like platinum particle. **d** High-resolution TEM image recorded from the boxed area marked in (**c**). The particles were prepared at −0.4 V for 100 s. The *scale bars* for (**a**), (**b**), (**c**), and (**d**) are 100 μm, 200 nm, 20 nm, and 1 nm, respectively

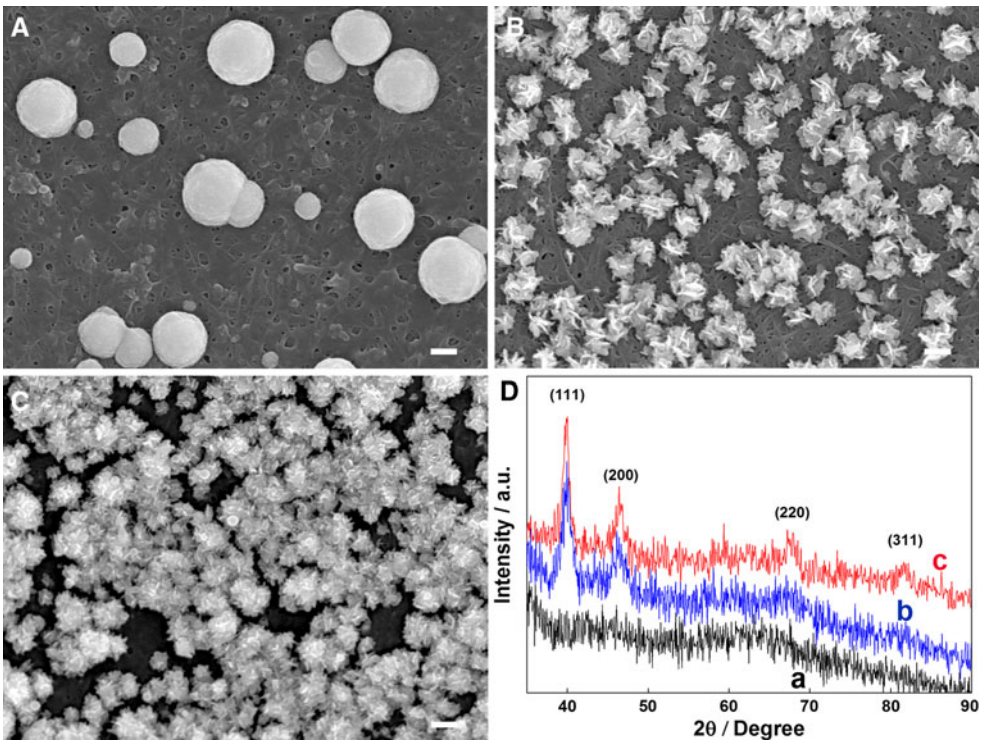

Fig. 3 FE-SEM images of the platinum particles obtained at different potentials. The applied potentials for **A**, **B**, and **C** were −0.2, −0.4, and −0.8 V, respectively. **D** X-ray diffraction patterns of (*a*) a bare SWCNT electrode, (*b*) a SPP-based electrode, and (*c*) a FPP-based electrode. Platinum particles were fabricated electrochemically on the SWCNT films with a pattern size of 100 × 100 μm; the *scale bars* are 200 nm

shown in the FE-SEM images of the platinum particles on the 100 × 100 μm SWCNT patterns in Fig. 3, different potentials were employed while the concentration of platinum ions and the electrodeposition time were held constant. At a potential of −0.2 V, spherical platinum particles (SPPs) with a diameter of approximately 400 nm were formed, but the density of the particles was low (Fig. 3A). When the electrodeposition potential was decreased to −0.4 V, the particle morphology changed from spherical to flower-like. The SWCNT film was covered with a highly dense array of FPPs with a diameter of approximately 200 nm (Fig. 3B). At a potential of −0.8 V, the reaction may have been too fast to separate the nucleation and growth processes, leading to FPP aggregation (Fig. 3C). These results indicate that higher potentials favor the fabrication of hierarchical FPPs with a high particle density. The XRD analysis of the FPPs revealed a face centered cubic (fcc) structure, as indicated by four peaks corresponding to the (111), (200), (220), and (311) crystal planes of the platinum (Fig. 3D). The intensity ratio of the (111) and (200) diffraction peaks of the FPPs (2.15) was greater than that observed for the SPPs (1.44), indicating the as-prepared FPPs were dominated by the lowest-energy (111) facets.

In addition to the applied potential, the pattern size of the SWCNT film also determines the morphologies and densities of the platinum particles. FE-SEM images of platinum particles on SWCNT electrodes with different pattern sizes are shown in Fig. 4. Platinum structures that were deposited electrochemically on a bare SWCNT film without patterns were spherical with diameters of approximately 300 nm (Fig. 4a). It is interesting to note that particles electrodeposited on SWCNT films with 0.5 × 0.5 cm square patterns underwent transitions from spheres to flower-like structures (Fig. 4b). On much smaller square patterns (100 × 100 μm), the particles were flower-like structures with a high density (Fig. 4c). On the bare SWCNT films, the strength of the electric field was uniform and homogeneous; however, on the patterned SWCNT films, the electric field strength was greater than that on the bare SWCNT surface and increased when the pattern size was reduced under the same potential [38]. Therefore, as the sizes of the patterns decreased, the density of the FPPs increased and the formation of flower-like microstructures was more likely because the FPPs were dominated by the lowest-energy (111) facets. The morphologies and densities of the platinum particles were adjusted by controlling the pattern sizes of the photoresist polymers during the photolithography step. To further assess the influence of deposition time, FPPs were grown on a 100 × 100 μm patterned SWCNT film. At deposition times of 50, 100, and 200 s, the obtained FPPs had diameters of approximately 150 nm, 200 nm, and 500 nm, respectively (Fig. S1, Supporting Information).

Based on these observations, the electron transfer reaction and crystallization (nucleation and growth) coexisted during the electrochemical synthesis of the platinum microstructures [40]. Platinum atoms (Pt^0) are first

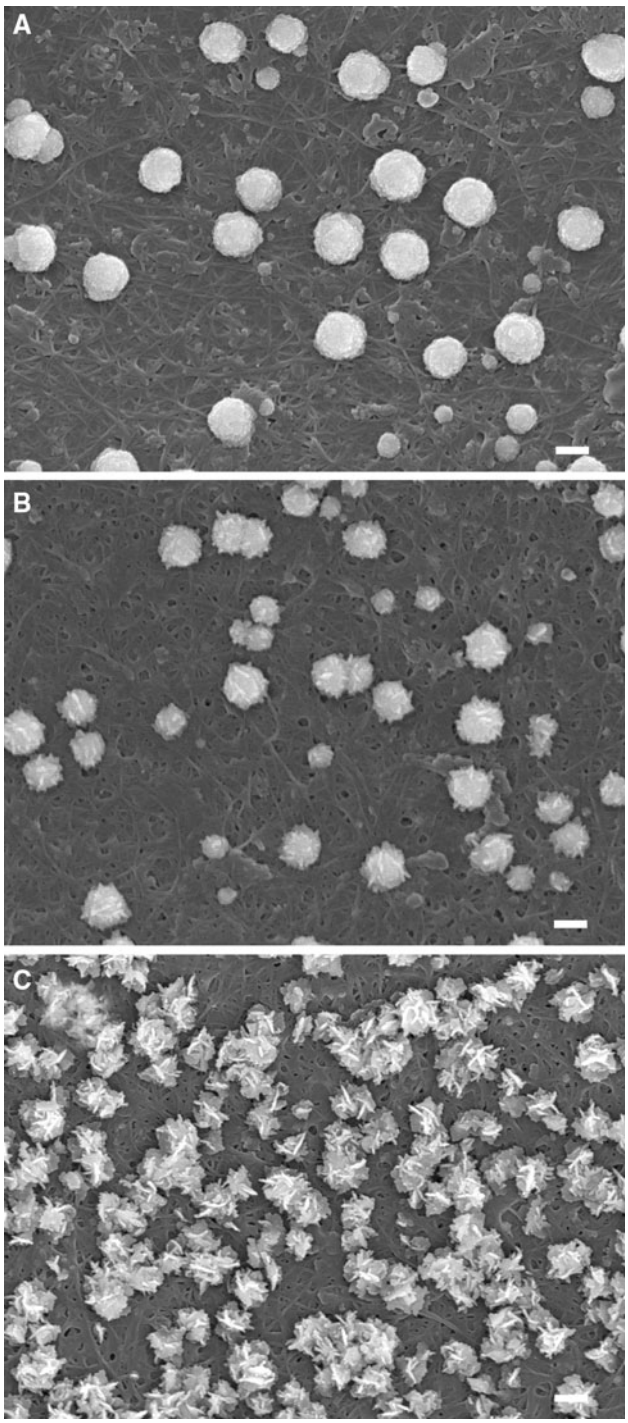

Fig. 4 FE-SEM images of platinum particles on SWCNT electrodes with different pattern sizes. The platinum particles were deposited on **a** bare SWCNT films, **b** large square-patterned SWCNT films (0.5 × 0.5 cm), and **c** small square-patterned SWCNT films (100 × 100 μm). The particles were prepared at −0.4 V for 100 s. The *scale bars* are 200 nm

produced on the SWCNT electrode through the reduction of $PtCl_6^{2-}$ via an electron transfer reaction. Platinum nuclei are then formed at stochastic positions on the surface and immediately aggregate to form core particles for secondary growth. The growth rates vary in different crystallographic directions, and the fast growth plane determines the final morphology. In fcc structures, the order of surface energies is (111) < (100) < (110) [41]. Cl^- ions play an important role in the growth process due to their preferential adsorption to certain facets. At high potentials and on small patterns, more Cl^- ions might be selectively adsorbed to a certain facet of platinum crystals. Therefore, selective interactions between Cl^- ions and the facet of platinum crystals lower the surface energy of the plane and hinder crystal growth perpendicular to this plane, resulting in a flower-like morphology [42]. However, at low potentials and on bare SWCNT films without patterns, nuclei will grow slowly and isotropically because the surface concentrations of Cl^- ions adsorbed to the platinum surfaces are low. This leads to the formation of spherical particles without preferential growth on certain facets [43]. While many 3D flower-like structures have been reported, the mechanism for the formation of particles through an interaction between primary particles remains a topic of debate among materials chemists.

Platinum particles exhibit catalytic activity for the electrochemical oxidation of methanol. Figure 5A provides CV results for methanol oxidation on a bare SWCNT electrode (curve a), a SWCNT electrode coated with SPPs (curve b), and a patterned SWCNT electrode with FPPs (curve c). It is apparent that both the SPP- and FPP-based SWCNT electrodes have significantly enhanced current densities compared to that of the bare SWCNT electrode, which has no electrocatalytic activity for the oxidation of methanol. An oxidation peak in the forward sweep was clearly observed at 0.72 V due to oxidation of methanol. In the backward sweep, the oxidation peak at 0.61 V was attributed to the oxidation of adsorbed CO or CO-like species, which were generated via incomplete oxidation of methanol in the forward scan [44]. All currents are reported per unit of electrochemically active surface area (ECSA), which was evaluated through the hydrogen adsorption/desorption region of CVs measured in a 0.5 M H_2SO_4 solution at a scan rate of 50 mV s^{-1} (Fig. S2, Supporting Information). The ECSA values of the SPP- and FPP-based SWCNT electrodes were 5.8 ± 0.5 and 6.7 ± 0.5 m^2 g^{-1}, respectively. The ECSA-normalized current density peaks of methanol oxidation on the FPP-based electrode were 0.143 and 0.089 mA cm^{-2} in the forward and backward sweeps, respectively. The corresponding peaks obtained on the SPP-based electrode were 0.078 and 0.051 mA cm^{-2} in the forward and backward sweeps, respectively.

Mass-normalized activity, which is another important parameter influencing the activity of surface atoms and Pt utilization [20], was also evaluated for the FPP- and SPP-based electrodes, and the values at the peak current in the

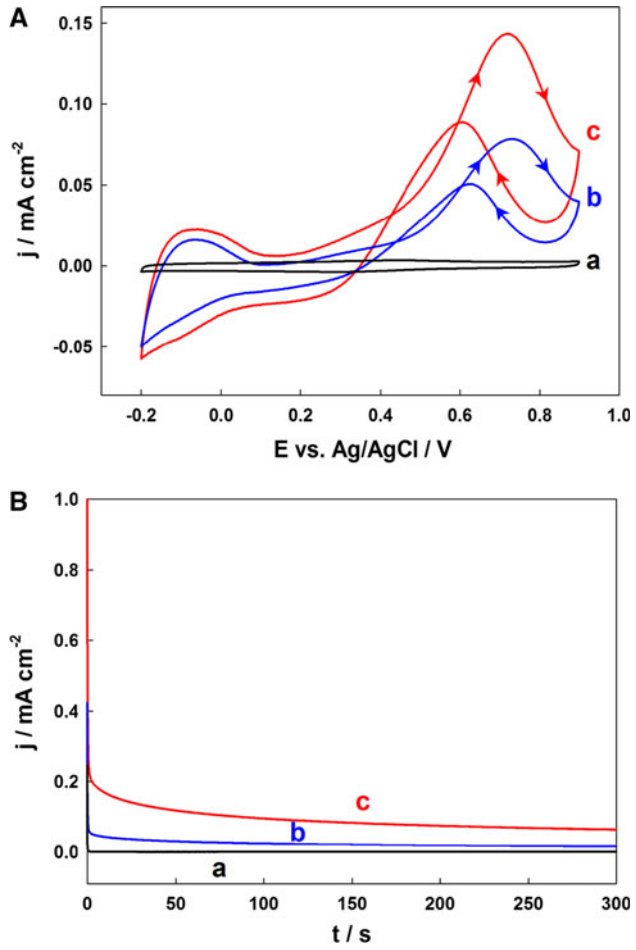

Fig. 5 **A** Cyclic voltammetry and **B** chronoamperometry results for (*a*) a bare SWCNT electrode, (*b*) a SPP-based electrode, and (*c*) a FPP-based electrode in 0.25 M methanol at a scan rate of 50 mV s^{-1}. The potential was held at −0.1 V for 60 s and then increased to 0.6 V. The current density, *j*, was normalized by the ECSA for each sample

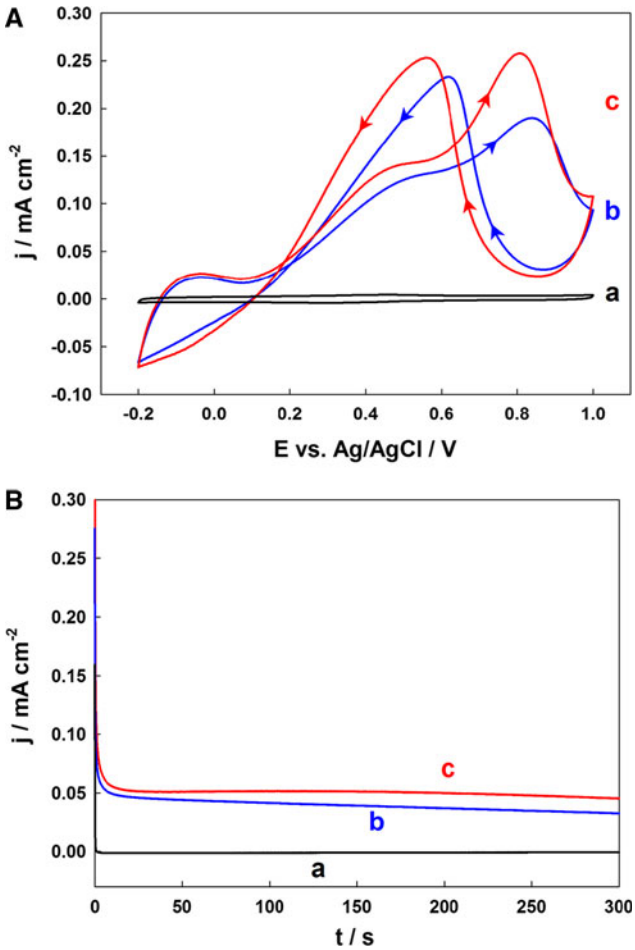

Fig. 6 **A** Cyclic voltammetry and **B** chronoamperometry results for (*a*) a bare SWCNT electrode, (*b*) a SPP-based electrode, and (*c*) a FPP-based electrode in 0.25 M formic acid at a scan rate of 50 mV s^{-1}. The potential was held at −0.1 V for 60 s and then increased to 0.4 V. The ECSA of each electrode was used to normalize the current density

forward sweep were 9.609 and 4.543 mA mg^{-1}, respectively (the amount of FPPs and SPPs on the SWCNT electrodes were 84 and 24 μg cm^{-2}, respectively). In addition, the ratio of the forward oxidation current peak (I_f) to the backward current peak (I_b), I_f/I_b, is an important index of the catalyst tolerance to poisoning species. A higher ratio indicates more effective removal of the poisoning species on the catalyst surface. The I_f/I_b ratio of the FPP-based SWCNT electrode was 1.61, which was greater than that of the SPPs (1.53), indicating the FPPs have higher catalyst tolerance (Fig. 5A). As shown in Fig. 5B, for current densities obtained after 300 s, the electrocatalytic performance of the FPP-based SWCNT electrode was better than that of the SPP-based SWCNT electrode with current density values of 63.88 and 15.34 μA cm^{-2}, respectively. The oxidation current density on the FPP-based electrode was much greater than that measured on the SPP-based electrode.

The electrocatalytic performance of the synthesized particles toward formic acid oxidation was also investigated. Figure 6A provides the CV results for formic acid oxidation on a bare SWCNT electrode (curve a), a SPP-based SWCNT electrode (curve b), and a FPP-based SWCNT electrode (curve c). Similar to the oxidation of methanol, both the FPP- and SPP-based SWCNT electrodes exhibited much higher currents than the bare SWCNT electrode. Two anodic peaks were observed in the forward sweep of the FPP-based SWCNT electrode. The first small anodic peak (∼0.45 V) was due to the direct oxidation of formic acid to carbon dioxide on the remaining sites unblocked by intermediate CO_{ads}. The second anodic peak is related to the oxidation of CO_{ads}, which releases the surface sites for the subsequent direct oxidation of formic acid. Based on the CV results, the electrochemical oxidation of formic acid on the platinum

particle-modified SWCNT electrode occurs through both dehydrogenation (to form the final product, CO_2) and dehydration (to form the intermediate, CO_{ads}). A large cathodic peak was observed on the backward sweep as most of the surface sites were free from occupation by the CO_{ads} and oxide species and were thus available for formic acid oxidation [45–47]. However, the anodic peaks of the FPP-based SWCNT electrode were larger and occurred at lower potentials than those of the SPP-based SWCNT electrode. Based on chronoamperometry measurements performed for 300 s, the current densities of the FPP- and SPP-based SWCNT electrodes were 45.27 and 38.23 $\mu A\ cm^{-2}$, respectively (Fig. 6B). The high oxidation current density observed for the FPP-based electrode was directly related to the platinum particle morphology.

4 Conclusions

In this study, 3D FPPs were fabricated directly on flexible, transparent SWCNT films using a simple electrochemical method. The size, shape, and uniformity of the platinum structures were effectively controlled by adjusting the applied potential, the pattern size of the photoresist polymer, and the deposition time. As-prepared FPPs exhibited good activities for the oxidation of both methanol and formic acid compared to those of the SPPs. The simple fabrication approach employed in this study will be useful for creating structures from other noble metals with different morphologies. Such structures could then be used in the fields of catalysis and biosensor development.

Acknowledgments This research was supported by a grant from the National Research Foundation (NRF) funded by the Korean government (MEST) (Nos. 2011-0015545 and 2010-0020638). We also acknowledge the financial support of the Ministry of Knowledge Economy (MKE) and the Korea Industrial Technology Foundation (KOTEF) through the Human Resources Training Project for Strategic Technology.

References

1. Grzelczak M, Correa-Duarte MA, Salgueiriño-Maceira V, Giersig M, Diaz R, Liz-Marzán LM (2006) Adv Mater 18:415
2. Liu J, Li X, Dai L (2006) Adv Mater 18:1740
3. Hu X, Dong S (2008) J Mater Chem 18:1279
4. Zeng S, Tang K, Li T, Liang Z (2007) J Colloid Interf Sci 316:921
5. Bell AT (2003) Science 299:1688
6. Heck RM, Farrauto RJ (2001) Appl Catal A Gen 221:443
7. Peng Z, Yang H (2009) Nano Today 4:143
8. Tian N, Zhou Z, Sun S (2008) J Phys Chem C 112:19801
9. Liang H, Zhang H, Hu J, Guo Y, Wan L, Bai C (2004) Angew Chem Int Ed 43:1540
10. Song Y, Garcia RM, Dorin RM, Wang H, Qiu Y, Shelnutt JA (2006) Angew Chem Int Ed 45:8126
11. Chen J, Lim B, Lee EP, Xia Y (2009) Nano Today 4:81
12. Tian N, Zhou Z, Sun S, Ding Y, Wang ZL (2007) Science 316:732
13. Demortiere A, Launois P, Goubet N, Albouy PA, Petit C (2008) J Phys Chem B 112:14583
14. Kijima T, Yoshimura T, Uota M, Ikeda T, Fujikawa D, Mouri S, Uoyama S (2004) Angew Chem Int Ed 43:228
15. Lin Z, Lin M, Chang H (2009) Chem Eur J 15:4656
16. Sun SH, Yang DQ, Villers D, Zhang GX, Sacher E, Dodelet JP (2008) Adv Mater 20:571
17. Zhong X, Feng Y, Lieberwirth I, Knoll W (2006) Chem Mater 18:2468
18. Mahmoud MA, Tabor CE, El-Sayed MA, Ding Y, Wang ZL (2008) J Am Chem Soc 130:4590
19. Lim B, Lu X, Jiang M, Camargo PHC, Cho EC, Lee EP, Xia Y (2008) Nano Lett 8:4043
20. Wang L, Yamauchi Y (2009) Chem Mater 21:3562
21. Teng X, Liang X, Maksimuk S, Yang H (2006) Small 2:249
22. Shen Q, Jiang L, Zhang H, Min Q, Hou W, Zhu J (2008) J Phys Chem C 112:16385
23. Song Y, Steen WA, Peña D, Jiang Y-B, Medforth CJ, Huo Q, Pincus JL, Qiu Y, Sasaki DY, Miller JE, Shelnutt JA (2006) Chem Mater 18:2335
24. Ullah MH, Chung W, Kim I, Ha C (2006) Small 2:870
25. Chen J, Herricks T, Xia Y (2005) Angew Chem Int Ed 44:2589
26. Ramirez E, Eradès L, Philippot K, Lecante P, Chaudret B (2007) Adv Funct Mater 17:2219
27. Xiao F, Zhao F, Mei D, Mo Z, Zeng B (2009) Biosens Bioelectron 24:3481
28. Kim J, Huang X, Choi Y (2008) J Phys Chem C 112:12747
29. Bui MN, Lee S, Han KN, Pham X, Li CA, Choo J, Seong GH (2009) Chem Commun 5549 (2009)
30. Girishkumar G, Rettker M, Underhile R, Binz D, Vinodgopal K, Mcginn P, Kamat P (2005) Langmuir 21:8487
31. Nikolou M, Dyer AL, Steckler TT, Donoghue EP, Wu Z, Heston NC, Rinzler AG, Tanner DB, Reynolds JR (2009) Chem Mater 21:5539
32. Zhou C, Kumar S, Doyle CD, Tour JM (2005) Chem Mater 17:1997
33. Wildgoose GG, Banks CE, Compton RG (2006) Small 2:182
34. Girishkumar G, Hall TD, Vinodgopal K, Kamat PV (2006) J Phys Chem B 110:107
35. Shim BS, Tang Z, Morabito MP, Agarwal A, Hong H, Kotov NA (2007) Chem Mater 19:5467
36. Sanles-Sobrido M, Correa-Duarte MA, Carregal-Romero S, Rodríguez-González B, Álvarez-Puebla RA, Hervés P, Liz-Marzán LM (2009) Chem Mater 21:1531
37. Wu Z, Chen Z, Du X, Logan JM, Sippel J, Nikolou M, Kamaras K, Reynolds JR, Tanner DB, Hebard AF, Rinzler AG (2004) Science 305:1273
38. Yang B, Lu N, Huang C, Qi D, Shi G, Xu H, Chen X, Dong B, Song W, Zhao B, Chi L (2008) Langmuir 25:55
39. Lu S, Panchapakesan B (2006) Appl Phys Lett 88:253107
40. Tang S, Meng X, Wang C, Cao Z (2009) Mater Chem Phys 114:842
41. Hoefelmeyer JD, Niesz K, Somorjai GA, Tilley TD (2005) Nano Lett 5:435
42. Guo S, Wang L, Wang E (2007) Chem Commun 3163 (2007)
43. Guo S, Fang Y, Dong S, Wang E (2007) Inorg Chem 46:9537
44. Mu Y, Liang H, Hu J, Jiang L, Wan L (2005) J Phys Chem B 109:22212
45. Wang J, Holt-Hindle P, MacDonald D, Thomas DF, Chen A (2008) Electrochim Acta 53:6944
46. Wang X, Hu JM, Hsing IM (2004) J Electroanal Chem 562:73
47. Lu GQ, Crown A, Wieckowski A (1999) J Phys Chem B 103:9700